Modelling of a GFRP adhesive connection by an imperfect soft interface model with initial damage

Aurelien Maurel-Pantel, Marco Lamberti, Maria Letizia Raffa, Camilo Suarez, Francesco Ascione, Frédéric Lebon

Modelling of a GFRP adhesive connection by an imperfect soft interface model with initial damage

A.Maurel-Pantel[a,*], M.Lamberti[a], M.L.Raffa[c], C.Suarez[a], F.Ascione[b], F.Lebon[a]

[a] *Aix Marseille Univ, CNRS, Centrale Marseille, LMA, Marseille, France*
[b] *Dept. of Civil Engineering, University of Salerno, Italy*
[c] *Supmeca, Laboratoire QUARTZ (EA 7393), Saint Ouen Cedex, France*

Abstract

In this paper a methodology to model a GFRP adhesive connections by using an imperfect soft interface model is presented. The model based on Kachanov's theory considered a cracked thin adhesive. Within this framework, the mechanical properties and the initial damage (diffuse initial cracks) of the adhesive layer has been experimentally evaluated. With a modified Arcan system, static tests were performed on adhesively bonded assemblies in tensile and shear solicitation mode considering three different adhesive thicknesses. The experimental results highlighted how the thickness of adhesive influences the mechanical strength and stiffness of the bonded connection. CT-scans were performed to measure the porosity rate in the adhesive layer. Furthermore, the excellent comparison of numerical and experimental data of an adhesive GFRP bonded connections allow us to consider the imperfect soft interface model proposed as highly competitive to evaluate complex structure performance in civil engineering context. A parametric analysis has been proposed to provide a formula able to describe the full response of the structure at varying adhesive property.

Keywords: Adhesive bonding, Imperfect interface model, GFRP connection, CT-scan, Damage, Porosity

2019 MSC: 00-01, 74S05, 74k30, 74R10

*Corresponding author
Email address: maurel@lma.cnrs-mrs.fr (A.Maurel-Pantel)

1. Introduction

During the last decade, the applications in the field of civil engineering of composite structures made of FRP (Fibre Reinforced Polymers) involving adhesives are grew exponentially due to the ability to tailor its structural performance, high axial resistance, high resistance to aggressive environment [1, 2, 3], considerably lightweight when compared to conventional materials, and quick installation time.

One of the most promising application is the realization of a beam-to-column connection by using structural adhesives that is becoming a valid alternative to the classical bolted connection. From nineties [4][5][6][7][8][9][10] to nowadays [11][12][13][14] beam-to-column connections were bolted and composed of I profiles based on the experience from steel applications. One of the principal drawback of these kind of connections is the bearing failure that limits the strength and stiffness.

On the contrary, in bonded connections due to the absence of holes, stresses are more uniformly distributed over the bonded surfaces. Indeed, the lack of holes avoid the presence of stress concentration, damage to the fibers and reduce the risk of moisture penetration in members. Moreover, adhesively bonded joints offer many advantages for the design of structures. But to improve the confidence that currently limits the use of this technology, several authors try to develop experimental [15][16][17] or numerical [18][19][20] approaches.

Recently, several experimental and numerical investigations were performed by some authors [21][22][23] to assess strength and stiffness of GFRP adhesive connection showing that their overall performance can match or overcome the performance of similar bolted connections in FRP structures. In the above mentioned papers the role of GFRP geometry was investigated varying the profiles adopted. In details, in [21][22] I-profiles (Fig.1(a)) were used for the beam and the column while in [23], a square tube was used for the column and U-profiles for the beam (built-up) as depicted in Fig.1(b). The first type of connection

(I-profiles) presented similar strength respect to the analogous bolted connections while the last one showed an increase in terms of strength and stiffness equal to 45%. If the overall mechanical response was deeply investigated, the

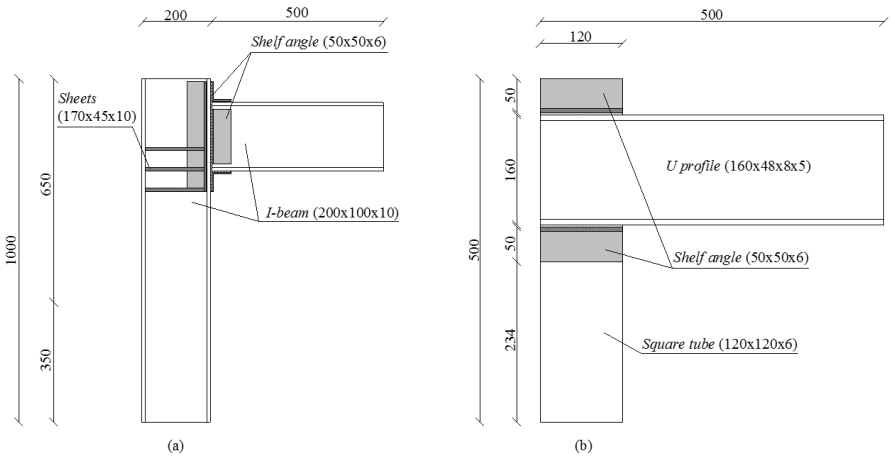

Figure 1: Homogeneous clamping device for the test samples

role of adhesive layer was not sufficiently studied. In particular, its thickness and its mechanical properties have to be deeply investigated in view of a further improvement of the mechanical response of such a bonded connection as well as for proposing design formulas.

The present paper proposes a methodology to model a GFRP adhesive connection in a complex structure by using an imperfect soft interface model (in the sense of [24] [25]) previously presented in [26]. In a first section a summary of previous experimental results obtained on a GFRP beam to column connection is proposed. Then in a second section the imperfect interface model is described. This model is derived by an asymptotic analysis [27] on a micro cracked adhesive based on Kachanov assumptions [28][29] successfully applied to composites materials [30, 31, 32]. The Kachanov theory consists to consider in a micro cracked adhesive the following main assumptions: a non interaction between the crack, a constant stress vector along the crack, and to ignore the

effect of the crack edge in the stress field. The choice of this model was done thanks to the possibility to take into account some bonding variabilities such as thickness variation, porosity, and initial damage. In a third section, experimental investigations are proposed in terms of adhesive stiffness and initial damage evaluation. Based on aforementioned experimental results, the interface model is enhanced. Finally the model is implemented in a finite element software and its validation is proposed comparing numerical results with those obtained experimentally[21].

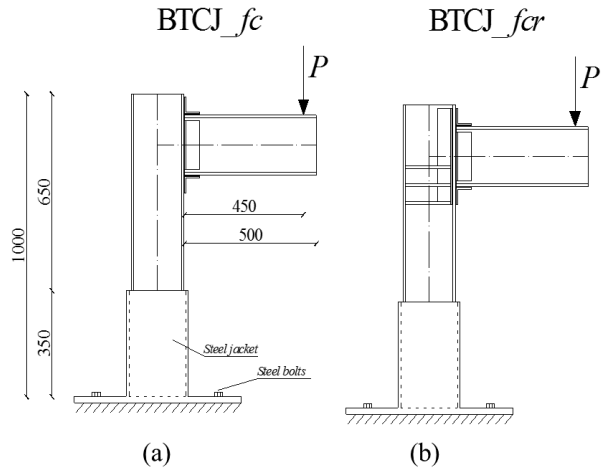

Figure 2: Details of the beam-to-column connections tested: (a) BTCj_fc, (b) BTCj_fcr.

2. GFRP Beam-to-column adhesive connection: experimental tests on complex structure

Some of the authors have experimentally investigated in a previous research program [21] the behavior of full-scale bolt-free GFRP beam-to-column connection under static load. Both the beam and the column had I-profile with dimensions of 200x100x10 mm. Four beam-to-column connection prototypes were tested varying the position of the connection respect to the column height and the strengthening system adopted. In all cases, the beam flanges and web

were bonded to the column compression flange by 50x50x6 mm seat angles. The connections which mechanical behavior is here numerically investigated are depicted in Fig.2. They have been originally designated as BTCJ_fc and BTCJ_fcr where BTCJ stands for Beam-to-Column Junction, fc for flange connection, the letter r for reinforced, respectively. More in detail, as shown in Fig.2(b), the strengthening system (to avoid premature failure of the column) consisted of pultruded GFRP strips (170x45x10 mm) and an angle at the column web/flange connection. The column can be considered fixed at the bottom with its unsupported length being 650 mm. To support the column at its bottom, it has been inserted inside a 350 mm high stiff steel jacket welded to a thick steel plate that was bolted to the testing machine platen (Fig.2). The beam was loaded monotonically in displacement control at a rate of 1 $mm.min^{-1}$ by a servo-controlled universal testing machine. The beam and column assembly was load by a point load applied near the free end of the beam at 450 mm from the beam-column flange connected to the beam (Fig.2). The experimental results are reported

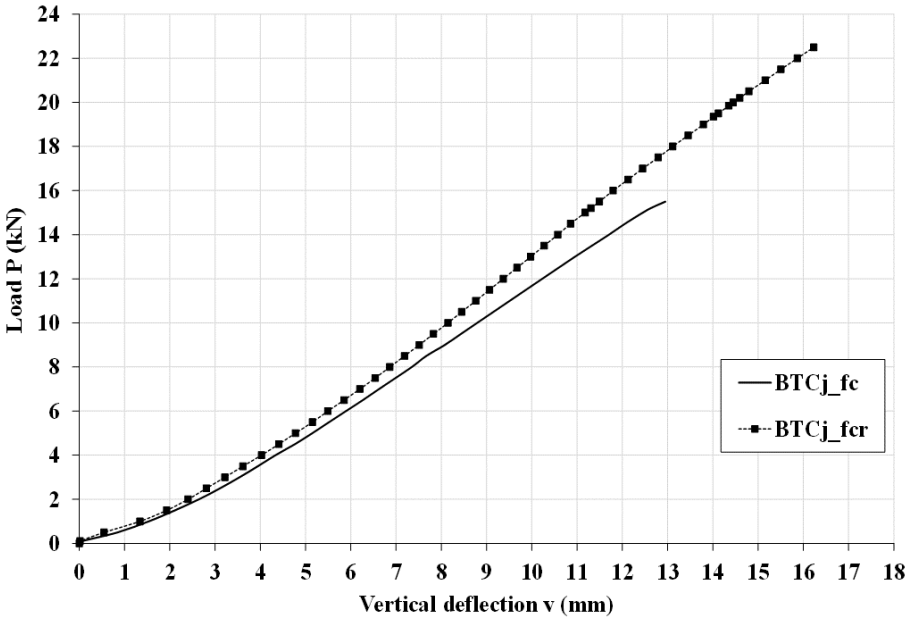

Figure 3: GFRP beam column experimental tests: Load-beam tip deflection.

in Fig.3 in terms of Load-beam vertical deflection. The latter is relative to the same cross-section where the load is applied. The connection exhibited basically a linear response up to failure. The un-strengthened connection reached a maximum applied load of 15.4 kN, while the strengthened one failed at about 23 kN. It must be pointed out that the deflection values in Fig.3 represent the deflection of the beam as a cantilever plus the deflection caused by the column end rotation, the local deformation of the column web and the joint rotation. All the graphs exhibit nonlinearity at low load levels, followed by a linear part and again ending with a nonlinear segment. The initial nonlinearity is the result of the specimen initial seating and not a characteristic of the connection.

3. Imperfect interface model

The proposed imperfect interface model coupling unilateral contact and damage is obtained via homogenization techniques and by an asymptotic approach within the small perturbations framework [27, 31]. The damaging behavior is modeled using the approach introduced in [26, 30, 32]: the thin glue interphase sandwiched between the two GFRP structures is assumed to be a microcracked material undergoing a degradation process. Each step of the proposed modeling strategy, sketched in Fig.5, is described below.

- Step 1: The real microstructure of the glue comprises various microcracks families with randomly distributed lengths and orientations. Within the non-interacting approximation [29] framework only one family of parallel microcracks which is representative of the macroscale behavior of the glue has been chosen denoting the equivalent length of microcracks family as l. Furthermore, the cracks orientation has been assumed parallel to the bonding plate.

- Step 2: The effective mechanical properties of the idealized microcracked material of Step 1 are obtained through a Kachanov-type homogenization technique [28, 29] based on the Eshelby's problem. The obtained elastic

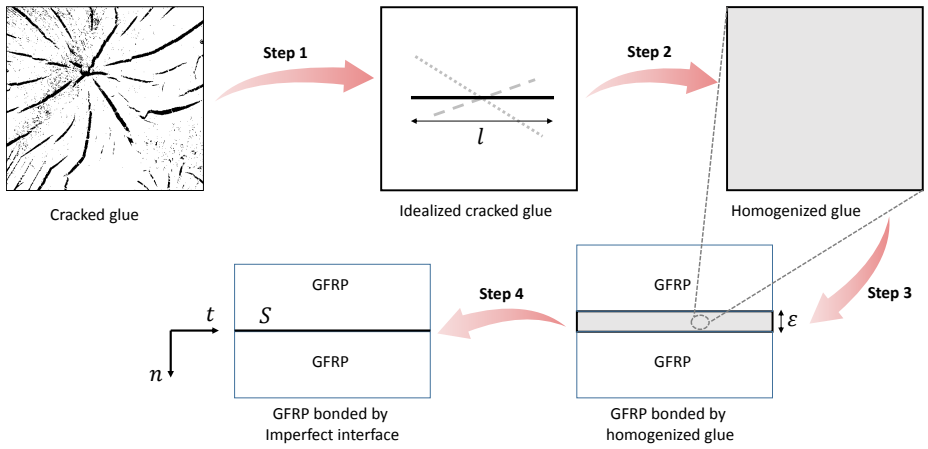

Figure 4: Imperfect interface modeling methodology

properties depend on the microcracks density ρ, which 3D form is $\rho = \dfrac{l^3}{V}$, V being the volume of the representative elementary domain. In section 4, it will be shown that l can be experimentally characterized. As an example, the Young's modulus in the normal-to-bonding plane direction E_N is equal to $\dfrac{E_0}{1+C\rho}$ where E_0 is the Young's modulus of the undamaged material and C is given by $\dfrac{16(1-\nu_0^2)}{3}$, where ν_0 is the Poisson ratio of the undamaged material. Note that the cracks density ρ can evolve thus it is representative of a damage parameter. An evolution law is introduced on l (or equivalently on ρ). To this purpose, the variation in time of l can be associated to a pseudo-potential of dissipation ϕ that is given by the sum of a quadratic term (rate-dependent) and a positively 1-homogeneous functional (rate-independent) [26]. The pseudo-potential of dissipation reads as: $\phi(\dot{l}) = \frac{1}{2}\eta\dot{l}^2 + I_{]0,\infty[}(\dot{l})$ where η is a positive viscosity parameter (which depends on the thickness of the glue) and I_B denotes the indicator function of a set B, i.e. $I_B = 0$ if $x \in B$ and $I_B = \infty$ otherwise. The term $I_{]0,\infty[}$ forces the crack length to assume non-negative values (i.e. the crack length can only increases) and renders the irreversible character of

the degradation process of the glue. In addition, the damage begins only if the elastic work is greater that a given value ω (which depends on the thickness of the glue) [26]. It is established that a Kachanov-type material is a *soft* material, i.e. the stiffness of the glue is of the same order as its thickness [33]. However, to impose unilateral contact (non-penetration condition) in the asymptotic expansions (Step 4), the glue is considered as a soft material only in traction (see first line of Equation (1)).

- Step 3: The homogenized material defined in step 2 is used to model a thin glue interphase of thickness ε. This interphase is sandwiched between two GFRP layers (denoted also adherents). We make the assumption that the bonding between the interphase and the adherents is perfect (i.e. continuity in interface separation and stress vector).

- Step 4: Using matching asymptotic expansions [27], the small parameter being the thickness of the glue, it is obtained at the limit that the interphase volume of the glue is replaced by an interface S of normal unit n (see fig. 5). More precisely, it is obtained a relationship across the surface S between the two adherents linking the stress vector σn and the interface separation $[u]$:

$$\begin{cases} \sigma n = K(l)\,[u]_+ + \tau \mathbf{n} & \text{on } S \\ \tau\,[u]\,.n = 0,\ \tau \leq 0,\ [u]\,.n \geq 0 & \text{on } S \\ \bar{\eta}\dot{l} = \left(\bar{\omega} - \frac{1}{2}K_{,l}(l)\,[u]_+\,.\,[u]_+\right)_+ & \text{on } S \end{cases} \tag{1}$$

where $()_{,l}$ denotes the partial derivative in l, $()_+$ is the positive part of a function, $[u]_+ = [u]$ if $[u]\,.n \geq 0$, $[u]_+ = [u] - [u]\,.n$ if $[u]\,.n \leq 0$. The parameter $\bar{\eta}$ (resp. $\bar{\omega}$) is the limit of $\eta\,\varepsilon$ (resp. $\omega\,\varepsilon$). Finally, as classically, K is the stiffness of the interface (the ratio between the stiffness of the glue and its thickness). Further details on asymptotic expansions, can be found in [27].

The interface constitutive law obtained in Equation (1) is a spring-like nonlinear interface model with a nonlinear evolution (i.e. damage) as related in Fig.5.

Note that the stiffness K keeps in memory the mechanical features of the original interphase (geometry, mechanical properties and damage).

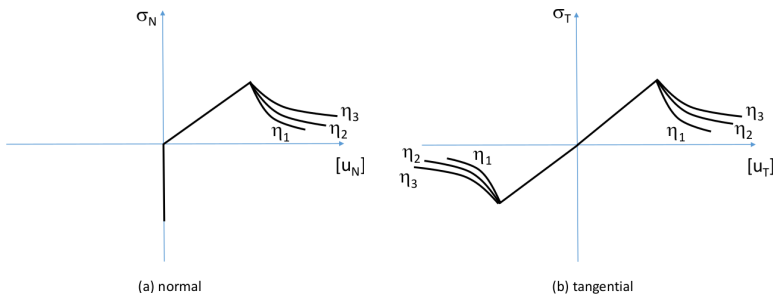

Figure 5: Interface constitutive law of the imperfect interface model proposed in Equation (1) for different values of $\bar{\eta}$. (a) normal stress component and (b) two tangential stress components.

4. Adhesive experimental characterization

4.1. Adhesive and Substrate

The adhesive used in experimental investigation [21] was the Sikadur-30 produced by Sika [34]. Such an adhesive is a 2-components thixotropic structural adhesive, a mixture of epoxy resin and special fillers, designed to bond at temperatures between 8° and 35°. The curing takes place in 7 days at room temperature. The properties of the glue given by the manufacturers are collected in Table 1. The substrates take the form of cylindrical specimens as depicted

SikaDur30		**Values (MPa)**	**Test standards**
Young Modulus	E_C	$9,600$	ASTM D695
	E_T	$11,200$	ISO 527
Compressive Strength	σ_C	$70-80$ (at $15°C$) et $85-95$ (at $35°C$)	EN 196
Tensile Strength	σ_N	$24-27$ (at $15°C$) et 26-31 (at $35°C$)	NF EN ISO 527-3
Shear Strength	σ_T	$14-17$ (at $15°C$) et 16-19 (at $35°C$)	FIP 5.15

Table 1: Properties of the epoxy adhesive (SikaDur-30) after 7 days of curing provided by manufacturers.[34]

in Fig.6. It is composed of Aluminum 2017 whose mechanical properties are summarized in the table 2. The aluminium samples are manufactured in such a way as to maintain a constant total height of the glued specimen equal to 64 mm. The total height includes the height of two half aluminum samples and the thickness of the adhesive joint as depicted in Fig.6. The samples are designed with a straight edge in order to have a homogeneous stress field at the interface in considering absence of defects.

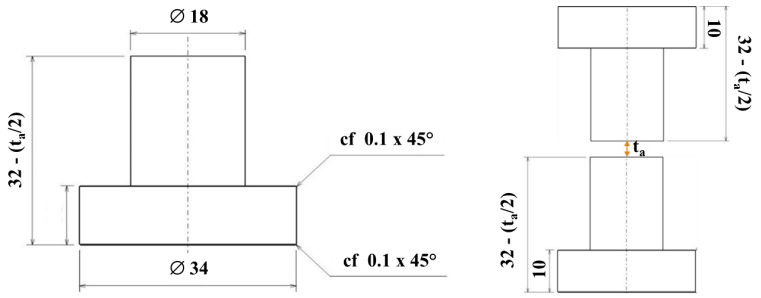

Figure 6: Cylindrical samples used for the mechanical tests.

$E(GPa)$	σ_y (MPa)	ν
70	210	0.3

Table 2: Material properties of the Aluminum 2017 provided by manufacturers.

4.2. Static tests based on Arcan device

Static tests are performed using the modified Arcan device [35]. This device permits to apply to adhesively bonded assembly different types of load. It is composed of two half discs with several attachment points along the perimeter. These attachment points allow setting up the device on a standard tensile testing machine. For the present investigation, the Arcan system was adapted to use cylindrical specimens. The positioning and the holding of the test sample are carried out using flanges. These flanges fix the sample with screws uniformly distributed on its periphery, which prevents the adhesive from being preloaded

(Fig.7). To keep a good stiffness gap, the half-discs are made of 40CMD8S Steel and the flanges of 7075 Aluminium. The static tests were carried out on a tensile

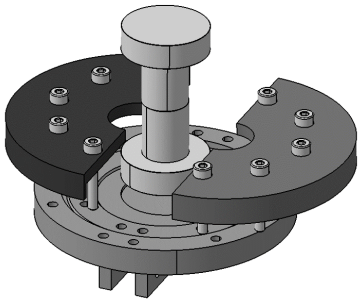

Figure 7: Homogeneous clamping device for the test samples.

test machine, an electromechanical Instron testing system (Fig.8). The Arcan device is connected to the machine with a ball joint that guarantees isostatism and alignment of the applied force. The tests were performed at a quasi-static speed of 0.5 $mm.min^{-1}$. The load is measured with a sensor with a capacity of 50 kN.

4.3. Bonding protocol

Three different adhesive joint thicknesses, noted t_a, have been tested: 1, 5, and 10 mm. For each test configuration, a minimum of five samples are tested to obtain an admissible statistic. In order to ensure the effectiveness of the bonding and to decrease dispersion, the aluminium surfaces was cleaned with acetone. To position the aluminium half samples and the adhesive, a mounting was designed as depicted in Fig.9. It allows to respect the coaxiality between the two aluminium half samples and has the advantage of being able to bond five samples at the same time. The half samples are placed on a lower base. The adhesive is applied to the bonding surfaces. The other half samples are placed on the upper base. The half samples are flanged in order to be attached to the base to facilitate positioning on other half samples. A guidance system allows the upper base to be positioned on the lower base and the half samples to

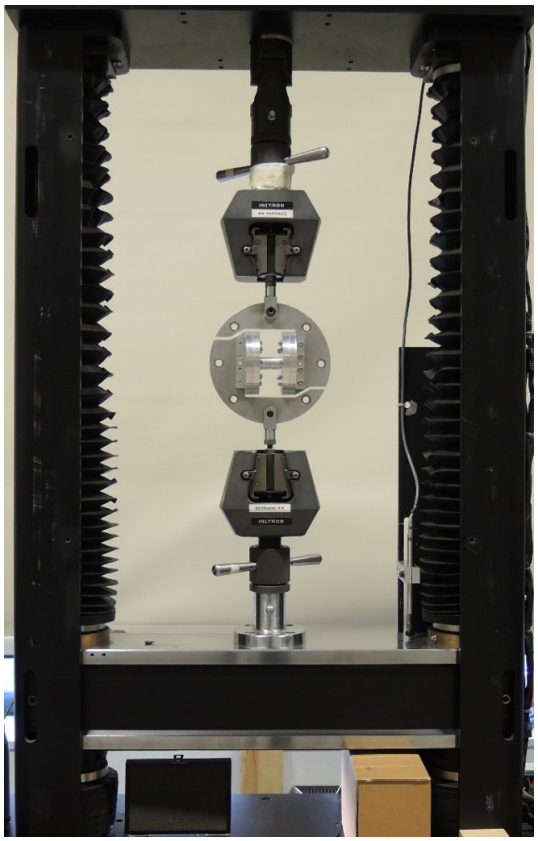

Figure 8: Arcan fixture is mounted in the Instron tensile machine.

be positioned relative to each other in calibrating the thickness. Once the test piece has been assembled, the glue joint must be gently cleaned, especially for thicker adhesive joints. Two examples of bonded specimens are shown in Fig.10. Then, it is necessary to wait for the polymerization of the adhesive which lasts 7 days at room temperature.

4.3.1. Tensile tests

In Fig.11, three of the total four graphs depict the stress-displacement curves obtained for a tensile loading for the three different adhesive thicknesses. In details, on the vertical axis the tensile stress and on the horizontal axis the normal displacement of the test machine are reported. For each test, the fracture

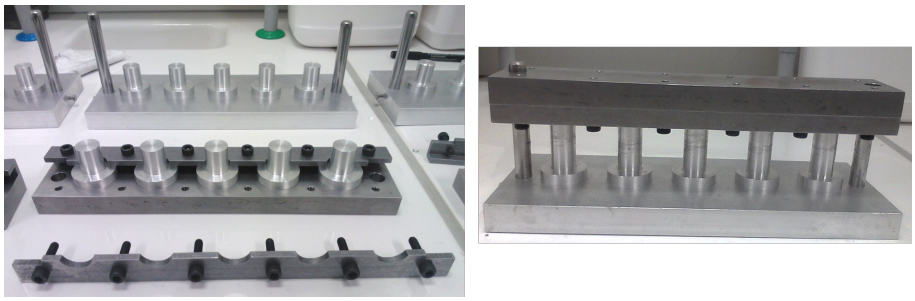

Figure 9: Mounting of samples to check the coaxiality and thickness of the adhesive joint.

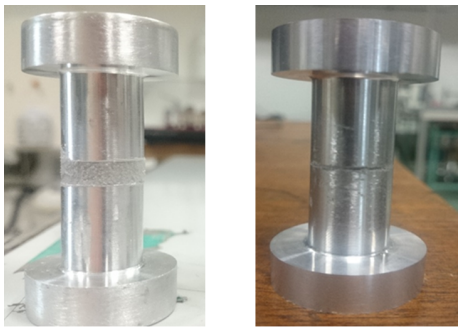

Figure 10: Two examples of bonded specimens.

was cohesive (i.e it means that the fracture occurred exclusively in the adhesive and not at the interface). The mechanical behaviour of the adhesive was linear with a brittle behaviour. In the test presented here, the contribution of the aluminum substrate to the measured stiffness is neglected, because the Young's modulus of the adhesive is 8 times lower than the modulus of the aluminum substrate. Results reported in Table 3 show that there is no dispersion on normal stiffness K_N^{exp} and normal critical stress at rupture σ_N^c over our five tests (the maximal coefficient of variation is less than 8.5%). It should be noted that the normal stiffness K_N^{exp} and the normal critical stress at fracture σ_N^c decrease as a function of adhesive thickness. In the forth graph of Fig.11, the stiffness of the interface has been plotted as a function of the thickness of the adhesive, and it can be seen that the stiffness decreases quasi-linearly as

a function of the thickness. The critical stress values are higher than those provided by the manufacturer, probably because we bond at an intermediate temperature ($24°C$) with extreme thickness values. Indeed, the manufacturer advises to use 3 mm and not to exceed 5 mm in thickness on vertical surfaces in order to avoid the collapse of the adhesive during the gluing process. In civil engineering context, one of the main difficulties is to control adhesive thickness (low thickness and low variability) for very large bonded surfaces.

Thickness t_a (mm)	K_N^{exp} Mean Value $(N.mm^{-3})$	K_N^{exp} RSD (%)	σ_N^c Mean Value (MPa)	σ_N^c CV (%)
1	86.57	7.31	31.84	1.81
5	85.41	5.12	26.22	8.32
10	79.25	2.21	25.38	2.54

Table 3: Tensile tests results: average values and relative standard deviation (RSD) of normal stiffness and normal stress for different thickness of the adhesive.

4.3.2. Shear tests

Similary to the case of tension test, in Fig.12 three of the total four graphs depict the stress-displacement curves obtained for a shear loading for the three different adhesive thicknesses. In details, on the vertical axis the shear stress and on the horizontal axis the displacement of the test machine are reported. For each test, the fracture was both cohesive and adhesive, these particular fracture surfaces observed are due to two successive shear phases: a pure shear phase followed by a mixed mode phase after the initiation of local fracture. As in tensile, the shear mechanical behaviour of the adhesive is linear with a brittle behaviour. Results reported in Table 4 show that tangential stiffness K_T^{exp} and tangential critical stresses at fracture σ_T^c over our five tests (the maximal coefficient of variation is less than 5%). As previously, the critical stress values are globally higher than those provided by the manufacturer. For 10 mm thickness, a smaller value is observed probably due to the limitation

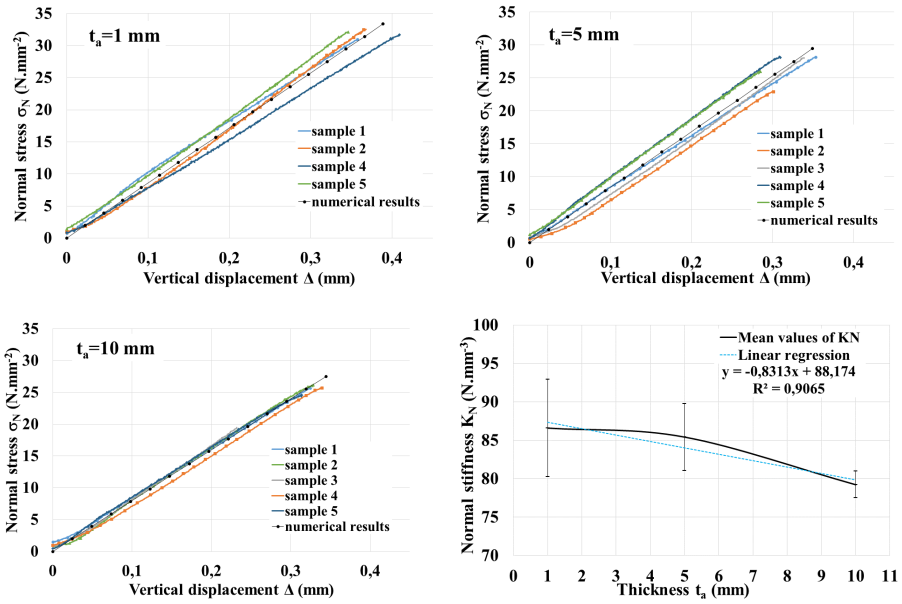

Figure 11: Experimental tensile tests results: Stress-displacement curves obtained for each thickness considered and Evolution of normal stiffness in function of the adhesive thickness. Numerical results of simulation of tensile tests with our imperfect interface model implemented in a finite element software.

of extreme thickness values in shearing configuration. It should be noted that the tangential stiffness K_T^{exp} and the tangential critical stress at rupture σ_T^c decreases with increasing adhesive thickness. In Fig.12, the stiffness of the interface has been plotted as a function of the adhesive thickness, and it can be seen that the stiffness decreases quasi-linearly as a function of the thickness. Globally, the same trends in tensile and in shear has been obtained.

4.4. CT-scan of the joint

The imperfect interface model assumes the description of initial damage by Kachanov's theory. For which the effect of a given number of diffuse cracks can be considered as the effect of a single large crack to describe the loss of bonding stiffness as a function of the initial cracking rate. In this section, the decrease of bonding stiffness is expressed as a function of thickness based on

Thickness t_a (mm)	K_T^{exp} Mean Value $(N.mm^{-3})$	K_T^{exp} RSD (%)	σ_T^c Mean Value (MPa)	σ_T^c CV (%)
1	20.5	4.71	23.71	2.28
5	19.73	1.65	19.17	0.21
10	17.22	4.76	15.13	1.52

Table 4: Shear tests results: average values and relative standard deviation (RSD) of tangential stiffness and tangential stress for different thickness of the adhesive.

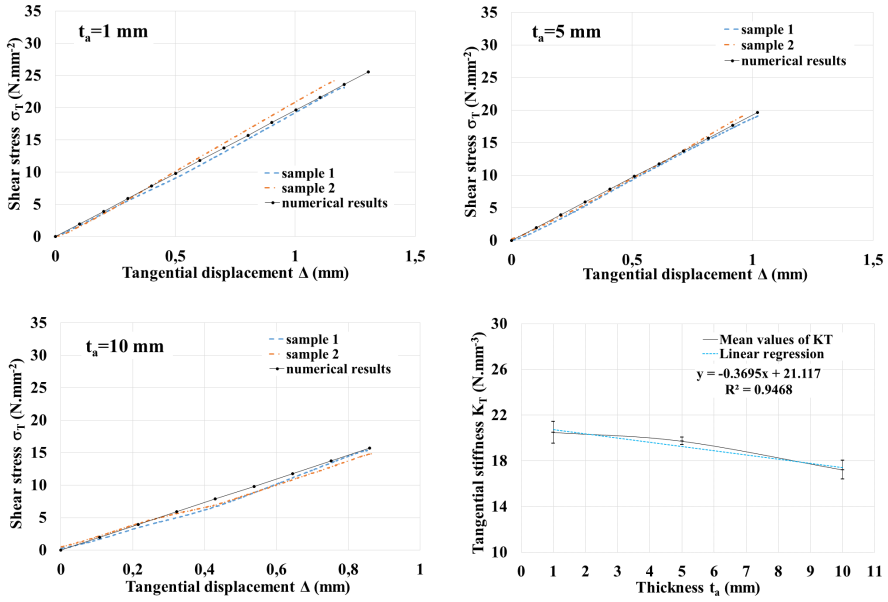

Figure 12: Experimental shear tests results: Stress-displacement curves obtained for each thickness considered and Evolution of tangential stiffness in function of the adhesive thickness. Numerical results of simulation of shear tests with our imperfect interface model implemented in a finite element software.

three-dimensional CT-scan of adhesive joints using an X-ray micro-tomograph. The adhesive joints are integrally scanned with a voxel size of 15 μm and a 1920 pixels x 1536 pixels resolution imager. The device used is an EasyTom XL Ultra 150 produced by RX Solution. The X-ray generator is a 150 keV sealed tube

with a minimum X-ray focus size of 5 μm and a maximum power of 75W. At the end of the reconstruction, each slice obtained has the thickness of a voxel. The Fig.13 allows to visualize the bonding defects, the pores with a low density appear in black, and the adhesive appears in grey level. Indeed, Sikadur-30 is a filled adhesive, on the slices of the Ct-scan the colloidal fillers can be seen in white and the binders in grey. On these slices, a diffuse porosity for each scanned adhesive joints and for each thickness considered is observed. Anyway, it is difficult to reach a conclusion by looking only at the slices obtained by microtomography. To get a more quantitative measurement, the stack of slices are uploaded to an open source analysis software developed by Vicente et al. and called Imorph[36][37]. This software allows to perform segmentation between pores and adhesive, in order to construct the boundary surfaces of the two phases and calculate a porosity rate ρ in the volume of the joint V. In Fig.14 the 3D reconstruction of pores obtained with the software is presented for the 1 mm adhesive joint. The number of pores seems very diffuse and quite important visually, the software is then able to quantify the volume of each phase. The values of the porosity rates calculated for the three thicknesses are reported in Table 5. The analogy with the Kachanov model allows us to correlate an initial damage length l_0 characteristic of the overall porosity volume l_0^3 (i.e. the sum of each porosity is equivalent to a single porosity of length l_0).

Thickness t_a (mm)	Volume of the joint V (mm^3)	Porosity rate $\rho = \frac{l_0^3}{V}$ (%)	Volume of porosity l_0^3 (mm^3)	Initial Damage Length l_0 (mm)
1	254.47	7.68	19.54	2.69
5	1272.35	8.02	102.04	4.67
10	2544.69	8.88	225.97	6.09

Table 5: Analysis of CT-scan measurements on initial samples bonded: Volume of porosity in function of the thickness of the adhesive.

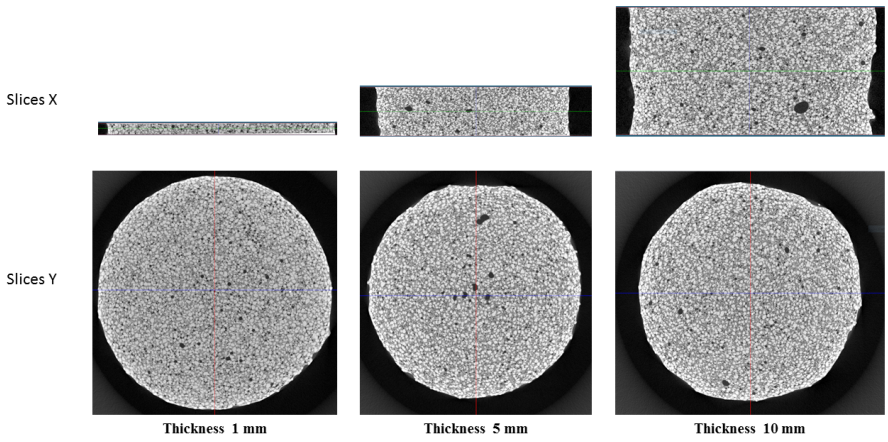

Figure 13: In situ 3D measurements: CT-scan Slices of adhesive joints.

Figure 14: 3D reconstruction of pores obtained with Imorph software [36][37].

4.5. Discussion on the model assumptions

Results of the experimental investigations allowed us to give an insight on the imperfect interface model proposed in section 3. Indeed, static tensile and shear tests showed that the normal and tangential stiffnesses of the interface decrease with the increase of the adhesive thickness as in Eq.1. 3D CT-scans demonstrates the possibility to correlate the decrease in stiffness with a porosity rate which can be considered as an initial damage. This parameter can be correlated to an initial damage length l_0 by analogy with Kachanov's theory. Table 5 describes a quasi-linear relation between the thickness and the initial damage length l_0 and Fig.15 describes a quasi-linear relation between the stiffness and l_0. The following expression can be proposed:

$$\begin{cases} K_N = f(thickness) = f(l_0) \\ K_T = f(thickness) = f(l_0) \end{cases} \tag{2}$$

In the imperfect interface model, the adhesive is characterized by an initial damage $l(t = 0) = l_0$. The value l_0 depends on the adhesive thickness used and the quality of bonding of the beam-to-column connection. On experimental results obtained with monotonic mechanical tests carried out on the beam-to-column connections described in Fig.3 and in static tests related in Fig.11 and in Fig.4, a brittle mechanical behavior of bonded connections is observed. It means that no significant damage evolution is observed in Sikadur30 adhesive. Thus, the connections is modeled with $\dot{l} = 0$ in Eq.1. This initial value is identified experimentally for the elementary samples and identified by inverse method for the GFRP adhesive connection.

5. Finite element simulations

The imperfect model presented in section 3, is implemented in the commercial finite element software COMSOL Multiphysics. In particular, both experimental tests on specimens for evaluating adhesive properties and on beam-to-column full scale specimens are simulated. Finally, comparisons between numerical and experimental investigation are performed.

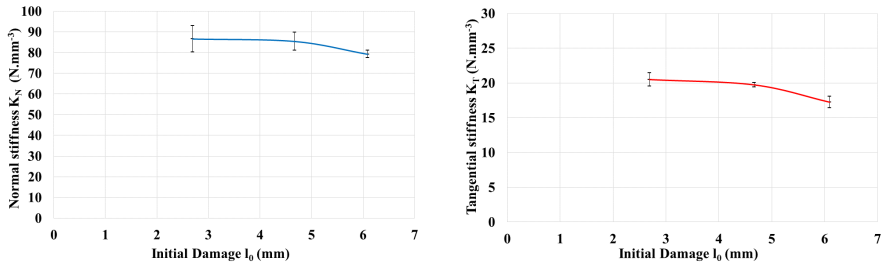

Figure 15: Stiffness of the adhesive joint in function of the initial damage l^0 measured with analysis of CT-scan measurements.

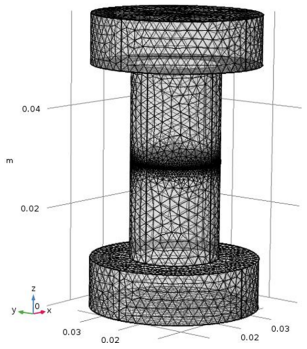

Figure 16: Mesh of the specimen tested in shear and tensile loadings.

5.1. Validation of the model on adhesive tests

Both the tensile and shear tests on the adhesive are simulated. Aluminum substrates are modelled by an isotropic linear elastic behaviour. The material parameters are reported in Table 2. The interface model which mechanical properties are collected in Table 2 provides the connection between the two substrates and describes the behaviour of the adhesive by integrating the effect of the adhesive thickness. The mesh of the specimen is described in Fig.16. After a mesh sensitivity study lead on the elastic response of the interface, the model includes 10,000 3D tetraedric elements, a finer mesh size (minimal 0.1 mm) is used at the interface. Boundary conditions correspond to experimental tests: the specimen is embedded on the plane surface noted A in Fig.16 and a displacement along the vertical axis is imposed on the plane surface noted B.

The numerical normal and tangential stiffnesses have been identified by comparison with experimental global response (see Fig.11 and Fig.4). The numerical stiffnesses identified are reported in Table 6. The maximal relative standard deviation on the normal stiffness is 1.24% and on the tangential stiffness is 6.21%. It is important to note that the differences between the experimental values and those identified numerically are very small confirming the assessment of the previous section.

Thickness (mm)	K_N^{num} $(N.mm^{-3})$	K_N^{exp} RSD (%)	K_T^{num} $(N.mm^{-3})$	K_T^{exp} RSD (%)
1	85.85	0.83	19.59	4.44
5	84.35	1.24	19.27	2.33
10	79.93	0.85	18.29	6.21

Table 6: Values and deviations from experimental values of tangential and normal stiffness for different thickness of the adhesive obtained by inverse identification based on finite element simulation of tensile and shear tests.

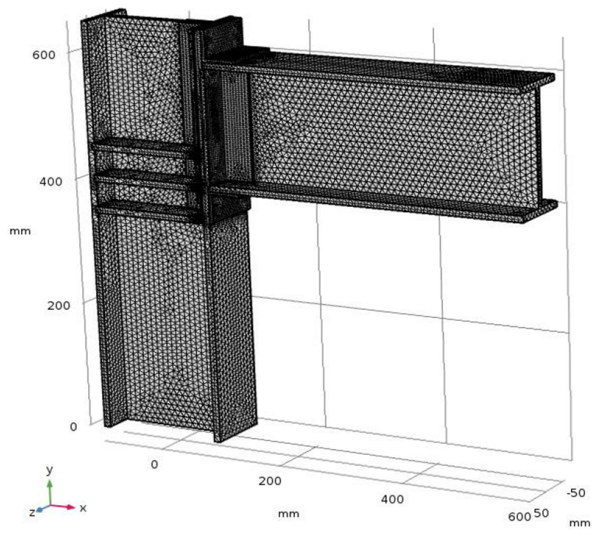

Figure 17: Mesh of the GFRP structure : beam to column connection reinforced (BTCJ_fcr).

Mechanical properties		measure unit	value
Young's modulus of elasticity	E_{0°	MPa	28,000
Young's modulus of elasticity	E_{90°	MPa	8,500
Shear modulus of elasticity	G	MPa	3,000
Poisson's ratio	ν_{0°	-	0.09
Poisson's ratio	ν_{90°	-	0.23

Table 7: Mechanical properties of GFRP pultruded laminates provided by the manufacturer.

5.2. Application of the model to GFRP beam-to-column connections

In order to validate the imperfect interface model and its efficiency to model a GFRP adhesive connection. Both complex structures of GFRP beam-to-column connection, depicted in Fig.2, are simulated using finite elements method. The GFRP panels are considered transversally isotropic which material parameters are reported in Table 7. The behaviour of the adhesive is described with the imperfect interface model where the adhesive stiffness depends of the damage variable l_0 as checked with the experimental analyses. The imperfect interface model framework presented in section 3, is applied at our parallelepipedic rectangular bonding thin interphase where L_1 is its large side, L_2 is its small side, and ε is its thickness. The homogenization of the adhesive and the asymptotic approach (from step 2 to step 4) lead to the following expression for the tangential and normal stiffness for a rectangular bonding interface [30][38]:

$$\begin{cases} K_N = f(l_0) = \frac{3E_T L_1 L_2}{16 l_0^3 (1-\nu^2)} \\ K_T = f(l_0) = \frac{3E_T L_1 L_2 (2-\nu)}{32 l_0^3 (1-\nu^2)} \end{cases} \tag{3}$$

where E_T is the tensile Young modulus of the adhesive as related in Table 1 and ν is the Poisson ratio. The adhesive thickness is constant and equal to 1 mm, thus, the value of l_0^3 is constant for all interface zones considered. This parameter has to be identified by inverse method for these specific GFRP adhesive connections. The mesh of the GFRP structure is described in Fig.17. The model includes 126,000 3D tetraedric elements, the mesh is refined at the bonding interface. The boundary conditions correspond to the test conditions:

the column is fixed at bottom and a displacement is imposed in the same cross section where the load was applied during experiments.

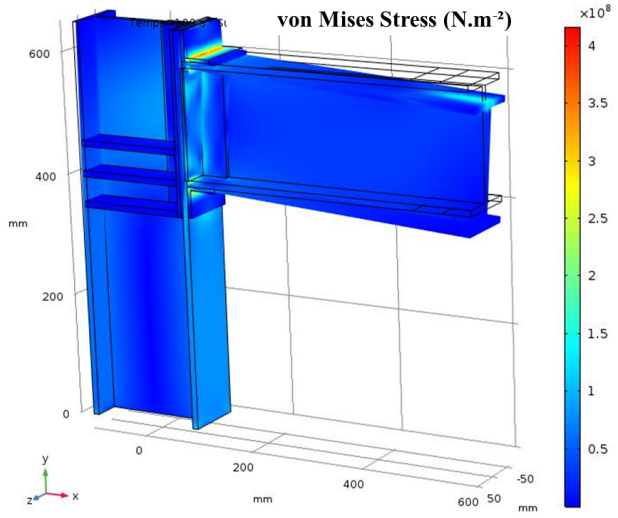

Figure 18: Numerical simulation results: deformed structure and von Mises stress field.

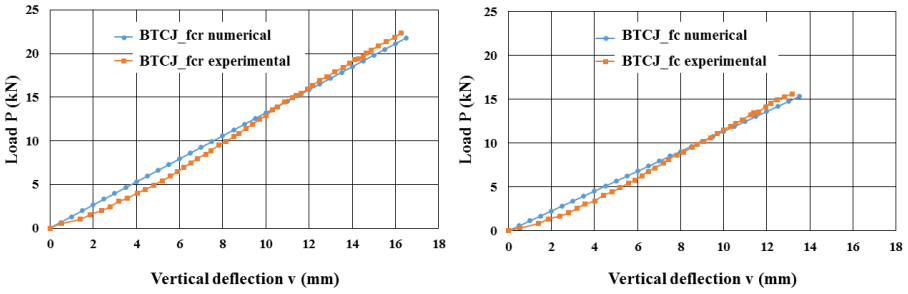

Figure 19: Comparison between numerical prediction and experimental results for both beam to column adhesive connection structures.

In Fig.18 the deformed structure and the von Mises stress field from the simulation results are reported for the reinforced BTCJ_fcr. It should be noted that numerical simulation gives a good prediction of the GFRP beam-to-column connections (see Fig.19). The l_0^3 value identified by inverse method is equal to 0.028 mm^3. The good agreement underline the capacity of the imperfect interface model to model this complex structures. Using this model, we are able

to propose formulas to design and verify bonded connections. For instance, the results summarized in Fig.20 allows to model the effect of the adhesive Young modulus on the vertical deflection of the GFRP beam-to-column adhesive connection BTCJ_fcr under a load applied equal to 15kN. On the basis of numerical results the following formula has been proposed in order to propose a first design rule of BTCJ_fcr structure:

$$v = aE^{-b} \tag{4}$$

with $a = 95.68$ and $b = -0.64$ identified on 8 different calculations with a excellent coefficient of correlation ($R^2 = 0.9948$). The parametric analysis is able to predict the nonlinear answer of the structure in taking into account the adhesive behavior included in the imperfect interface model.

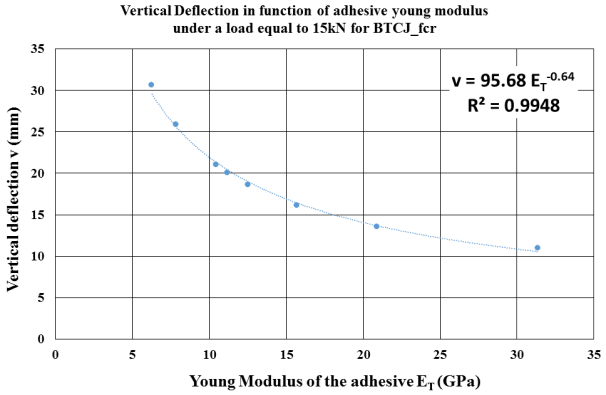

Figure 20: Variation of the vertical deflection of GFRP beam to column adhesive connection BTCJ_fcr in function of the Young modulus of the adhesive.

6. Conclusions

The mechanical properties of a structural adhesive available on the market has been experimentally evaluated by means of modified Arcan device. A monotonic load was applied on the adhesive bonded assembly. The results obtained by experimental tests have permitted to model a GFRP adhesive connection of a complex structures by using an imperfect soft interface model previously presented by some of the authors. The results of the study support the following conclusions:

1) The thickness of adhesive layers influences significantly interface mechanical properties. In particular in reducing the thickness from 10 to 1 mm, it is possible to obtain an increase of 25% and 8% in terms of normal strength and stiffness, and an increment of 57% and 19% in terms of tangential strength and stiffness. Furthermore, the adhesive presents a brittle mechanical behavior and an initial damage (i.e an initial porosity rate in Kachanov's theory) depending of the geometry, the thickness of the joint and the bonded GFRP structure considered.

2) Results of the experimental investigations on elementary samples allowed us to give an insight on the imperfect interface model. The CT-scan demonstrated that is possible to correlate the decrease in stiffness with a porosity rate or initial damage. This parameter being correlated to an initial damage length l_0 by analogy with Kachanov theory. Numerical results of elementary tests are in very good agreement with experimental ones.

3) The results of imperfect interface model are in very good agreement with the experimental results of a bonded GFRP connection previously tested by the authors. The imperfect interface model is considered as an useful instrument to study the performance of GFRP adhesive connection in civil engineering context.

4) A parametric analysis have been undertaken in order to define a new formula able to describe the nonlinear response of the bonded connection in terms of vertical deflection at varying of adhesive property.

After the first encouraging results, the next goal for the authors will be the investigation of the influence of adhesive mechanical properties on cyclic behaviour with particular attention on damage evolution. It will be possible in the future to reactivate the $\dot{l}$ parameter in order to describe the mechanical response of these connections to cyclic solicitations (loads/unloads) or connections with different geometries.[23]

Acknowledgement

This project has received funding from the European Union Horizon 2020 research and innovation programme under the Marie Sklodowska-Curie grant agreement No 843218-ASSO (Adhesive connection for Secondary Structures in Offshore wind installations).

References

References

[1] J. R. Correia, GFRP pultruded profiles in civil engineering: hybrid solutions, bonded connections and fire behaviour, Lisboa: Tese de Doutoramento em Engenharia Civil, Instituto Superior Técnico-Universidade Técnica de Lisboa.

[2] K. Liao, C. Schultheisz, D. L. Hunston, Effects of environmental aging on the properties of pultruded GFRP, Composites Part B: Engineering 30 (5) (1999) 485–493.

[3] S. Cabral-Fonseca, J. Correia, M. Rodrigues, F. Branco, Artificial accelerated ageing of GFRP pultruded profiles made of polyester and vinylester resins: characterisation of physical–chemical and mechanical damage, Strain 48 (2) (2012) 162–173.

[4] A. S. Mosallam, M. K. Abdelhamid, J. H. Conway, Performance of pultruded FRP connections under static and dynamic loads, Journal of Reinforced Plastics and Composites 13 (5) (1994) 386–407.

[5] L. C. Bank, A. S. Mosallam, G. T. McCoy, Design and performance of connections for pultruded frame structures, Journal of Reinforced Plastics and Composites 13 (3) (1994) 199–212.

[6] L. C. Bank, J. Yin, L. Moore, D. J. Evans, R. W. Allison, Experimental and numerical evaluation of beam-to-column connections for pultruded structures, Journal of Reinforced Plastics and Composites 15 (10) (1996) 1052–1067.

[7] S. Smith, I. Parsons, K. Hjelmstad, An experimental study of the behavior of connections for pultruded GFRP I-beams and rectangular tubes, Composite Structures 42 (3) (1998) 281–290.

[8] S. Smith, I. Parsons, K. Hjelmstad, Experimental comparisons of connections for gfrp pultruded frames, Journal of Composites for Construction 3 (1) (1999) 20–26.

[9] J. Mottram, Y. Zheng, Further tests on beam-to-column connections for pultruded frames: Web-cleated, Journal of Composites for Construction 3 (1) (1999) 3–11.

[10] J. Mottram, Y. Zheng, Further tests of beam-to-column connections for pultruded frames: flange-cleated, Journal of Composites for Construction 3 (3) (1999) 108–116.

[11] J. Qureshi, J. T. Mottram, Behaviour of pultruded beam-to-column joints using steel web cleats, Thin-Walled Structures 73 (2013) 48–56.

[12] J. Qureshi, J. T. Mottram, Response of beam-to-column web cleated joints for FRP pultruded members, Journal of Composites for Construction 18 (2) (2013) 04013039.

[13] A. Mosallam, Design Guide for FRP Composite Connections, American Society of Civil Engineers, 2011. doi:10.1061/9780784406120.

[14] M. Lamberti, M. Maurel-Pantel, F. Ascione, F. Lebon, Influence of web/flange reinforcement on the GFRP bonded beams mechanical response: A comparison with experimental results and a numerical prediction, Composite Structures 147 (2016) 247–259.

[15] S. Chataigner, J.-F. Caron, K. Benzarti, M. Quiertant, C. Aubagnac, Use of a single lap shear test to characterize composite-to-concrete or composite-to-steel bonded interfaces, Construction and Building Materials 25 (2) (2011) 468–478. doi:10.1016/j.conbuildmat.2010.08.009.

[16] G. Bresson, J. Jumel, M. E. Shanahan, P. Serin, Strength of adhesively bonded joints under mixed axial and shear loading, International Journal of Adhesion and Adhesives 35 (2012) 27–35. doi:10.1016/j.ijadhadh.2011.12.006.

[17] J. Jumel, N. B. Salem, M. K. Budzik, M. E. Shanahan, Measurement of interface cohesive stresses and strains evolutions with combined mixed mode crack propagation test and backface strain monitoring measurements, International Journal of Solids and Structures 52 (2015) 33–44. doi:10.1016/j.ijsolstr.2014.09.004.

[18] F. Freddi, E. Sacco, An interphase model for the analysis of the masonry-FRP bond, Composite Structures 138 (2016) 322–334. doi:10.1016/j.compstruct.2015.11.041.

[19] C. Sarrado, F. A. Leone, A. Turon, Finite-thickness cohesive elements for modeling thick adhesives, Engineering Fracture Mechanics 168 (2016) 105–113. doi:10.1016/j.engfracmech.2016.03.020.

[20] A. Maurel-Pantel, M. Voisin, Q. Bui, N. Cocheteau, F. Lebon, C. Hochard, A cohesive zone model for fracture initiation and propagation of fused silica direct bonding interface, Engineering Fracture Mechanics 219 (2019) 106649. doi:10.1016/j.engfracmech.2019.106649.

[21] F. Ascione, M. Lamberti, A. Razaqpur, S. Spadea, Strength and stiffness of adhesively bonded GFRP beam-column moment resisting connections, Composite Structures 160 (2017) 1248–1257.

[22] F. Ascione, M. Lamberti, A. Razaqpur, S. Spadea, M. Malagic, Pseudo-ductile failure of adhesively joined GFRP beam-column connections: An experimental and numerical investigation, Composite Structures 200 (2018) 864–873.

[23] G. Razaqpur, F. Ascione, M. Lamberti, S. Spadea, M. Malagic, GFRP hollow column to built-up beam adhesive connection: Mechanical behaviour under quasi-static, cyclic and fatigue loading, Composite Structures 224 (2019) 111069.

[24] Y. Benveniste, T. Miloh, Imperfect soft and stiff interfaces in two-dimensional elasticity, Mechanics of Materials 33 (6) (2001) 309–323. doi:10.1016/s0167-6636(01)00055-2.

[25] Z. Hashin, Thermoelastic properties of fiber composites with imperfect interface, Mechanics of Materials 8 (4) (1990) 333–348. doi:10.1016/0167-6636(90)90051-g.

[26] E. Bonetti, G. Bonfanti, F. Lebon, R. Rizzoni, A model of imperfect interface with damage, Meccanica 52 (2017) 1911–1922.

[27] F. Lebon, R. Rizzoni, Asymptotic behavior of a hard thin linear elastic interphase: an energy approach, International Journal of Solids and Structures 49 (2011) 441–449.

[28] I. Tsukrov, M. Kachanov, Effective moduli of an anisotropic material with elliptical holes of arbitrary orientational distribution, International Journal of Solids and Structures 69 (2000) 5919–5941.

[29] I. Sevostianov, M. Kachanov, On some controversial issues in effective field approaches to the problem of the overall elastic properties, Mechanics of Materials 69 (2014) 93–105.

[30] M. L. Raffa, F. Lebon, R. Rizzoni, Derivation of a model of imperfect interface with finite strains and damage by asymptotic techniques: an application to masonry structures, Meccanica 53 (2018) 1645–1660.

[31] A. Rekik, F. Lebon, Homogenization methods for interface modeling in damaged masonry, Advances in Engineering Software 46 (2012) 35–42.

[32] A. Orefice, G. Mancusi, S. Dumont, F. Lebon, Experimental/numerical study on the interfacial damage of bonded joints for fibre-reinforced polymer profiles at service conditions, Technologies 4 (2016) in line.

[33] M. L. Raffa, F. Lebon, G. Vairo, Normal and tangential stiffnesses of rough surfaces in contact via an imperfect interface model, International Journal of Solids and Structures 87 (2016) 245–253.

[34] SikaDur30 technical data sheet (2020).
URL http://fra.sika.com/dms/getdocument.get/f87e83b7-c0c8-3d69-b5ad-8ac164d9be05/sikadur_30_nt3022.pdf

[35] J. Cognard, P. Davies, B. Gineste, L. Sohier, Development of an improved adhesive test method for composite assembly design, Composites Science and Technology 65 (3-4) (2005) 359–368. doi:10.1016/j.compscitech.2004.09.008.
URL http://linkinghub.elsevier.com/retrieve/pii/S0266353804002131

[36] J. Vicente, Y. Wyart, P. Moulin, Characterization (2d-3d) of ceramic microfiltration membrane by synchrotron radiation: new and abraded membranes, Journal of Porous Media 16 (6) (2013) 537–545. doi:10.1615/jpormedia.v16.i6.50.

[37] C. El Hachem, K. Abahri, J. Vicente, R. Bennacer, R. Belarbi, Hygromorphic characterization of softwood under high resolution X-ray tomography for hygrothermal simulation, Heat and Mass Transfer 54 (9) (2018) 2761–2769.

[38] M. L. Raffa, Micromechanical modeling of imperfect interfaces and applications, Ph.D. thesis, Aix-Marseille Universite, Universita di Roma Tor Vergata (2015).